Mapping the Magnetostructural Quantum Phases of Mn_3O_4

M. Kim, X. M. Chen, Y. I. Joe, E. Fradkin, P. Abbamonte, and S. L. Cooper

Department of Physics and Frederick Seitz Materials Research Laboratory, University of Illinois, Urbana, Illinois 61801, USA

(Received 9 December 2009; published 30 March 2010)

We present temperature-dependent x-ray diffraction and temperature- and field-dependent Raman scattering studies of single-crystal Mn_3O_4, which reveal the magnetostructural phases that evolve in the spinels due to the interplay between strong spin-orbital coupling, geometric frustration, and applied magnetic field. We present evidence that the magnetoelastic and magnetodielectric behavior in this material is governed by magnetic-field-controlled tetragonal-to-monoclinic phase changes. Most interestingly, for an applied field transverse to the ferrimagnetic ordering direction, $\mathbf{H} \parallel [1\bar{1}0]$, we find evidence for a field-tuned quantum phase transition to a tetragonal spin-disordered phase, indicating that a structurally symmetric, spin frustrated phase can be recovered at $T \sim 0$ for intermediate transverse fields in Mn_3O_4.

DOI: 10.1103/PhysRevLett.104.136402 PACS numbers: 71.70.Ej, 73.43.Nq, 78.30.−j

The development at low temperatures of some form of long-range order—such as magnetism, orbital-order, charge-order, or superconductivity—is ubiquitous in materials [1], and reflects the tendency of a material to lower its ground state degeneracy and minimize its entropy near $T = 0$ K. Recently, there has been substantial interest in materials in which atomic geometry, competing interactions, and applied fields conspire to ''frustrate'' the onset of long-range magnetic and/or orbital order, even down to $T = 0$. Frustrated systems are of interest because of the novel low temperature phase behavior they have been proposed to exhibit—including orbital [2,3] and spin liquids and glasses [4,5], and spin-ice states [6]—and because of the opportunity they provide to study how quantum fluctuations impact low temperature phases of materials [7].

One of the prototypical materials families that exhibit orbital frustration and spin frustration are the spinels, in which strong interactions and geometrical frustration result in a rich variety of exotic magnetic and structural phases among family members: sulfur-based spinels such as FeB_2S_4 (B = Cr, Sc) exhibit orbital-liquid or -glass ground states; [3–5] the chromium-oxide spinels AB_2O_4 (A = Zn, Cd, Hg; B = Cr) exhibit three-dimensional spin-Peierls transitions involving coupled magnetic and structural transitions [8]; and the vanadium-oxide spinels AB_2O_4 (A = Zn, Cd, Mn; B = V) display complex spin-orbital ordering and large magnetoelastic and magnetodielectric effects [9,10]. The frustration and diversity of low temperature phase behavior in the spinels is believed to be governed primarily by the interplay between spin-orbital coupling, applied field, and frustrated exchange interactions [7]. However, there has been little experimental investigation of the microscopic details of this interplay.

In this Letter, we study the temperature- and field-dependent magnetostructural phases of the spinel Mn_3O_4 using a combination of Raman spectroscopy and x-ray scattering. In spite of its simpler chemical composition—with Mn ions at both tetrahedral ($A = Mn^{2+}$) and octahedral ($B = Mn^{3+}$) sites—Mn_3O_4 exhibits the rich magnetostructural transitions characteristic of more complex ternary magnetic spinels: this includes ferrimagnetic ordering below $T_C = 43$ K, in which the net spin of the octahedrally coordinated Mn^{3+} spins is antiparallel to the [110] direction of the tetrahedrally coordinated Mn^{2+} spins [10,11]; incommensurate spin ordering of the Mn^{3+} spins below $T_1 = 39$ K; and commensurate ferrimagnetic ordering below $T_2 = 33$ K, in which the net Mn spins are oriented in the [110] direction and the magnetic unit cell doubles the chemical unit cell [11,12]. Our studies of this simple spinel illustrate the importance of magnetoelastic energies—which have been largely ignored in theoretical investigations—in governing the low temperature phase behavior of the spinels. Of particular interest is the discovery of a quantum ($T \sim 0$) phase transition to a structurally isotropic, disordered spin-orbital state for magnetic fields applied *transverse* to the ferrimagnetic moments, i.e., for $\mathbf{H} \parallel [1\bar{1}0]$, which demonstrates the important role that magnetoelastic interactions can play in frustrating spin and orbital order at $T = 0$.

A single-crystal sample of Mn_3O_4 was grown at the University of Illinois using a floating zone technique. Field-dependent Raman measurements were performed as described previously [13] on an as-grown surface of single-crystal Mn_3O_4 with surface normal along the easy-axis [110] direction. Temperature-dependent x-ray measurements were carried out on the as-grown [110] surface of Mn_3O_4 using Mo K_α radiation from a Rigaku rotaflex RU-300 rotating anode source. A graphite (004) monochromator was employed to remove Bremsstrahlung from the source, and an energy-resolving, solid state detector was used with a multichannel analyzer to reject sample fluorescence. A closed cycle He refrigerator was used to control the sample temperature. A Phillips MRD X'Pert

system was used for high precision measurements at room temperature. A least squares program was used to determine the lattice parameters of the crystal from the data.

The room-temperature Raman spectrum of our Mn_3O_4 sample exhibits 5 phonon peaks, consistent with previous reports [14]: a T_{2g} symmetry mode at 290 cm^{-1}, an E_g symmetry mode at 320 cm^{-1}, T_{2g} symmetry modes at 375 and 479 cm^{-1}, and an A_{1g} symmetry mode at 660 cm^{-1}. In this Letter, we focus on the lowest energy T_{2g} phonon mode, which involves Mn-O bond-stretching vibrations of the tetrahedral site ions [14].

Figure 1(b) shows the temperature dependence of the T_{2g} mode intensity and the T_{2g} mode energy and linewidth for light polarized along the $[1\bar{1}0]$ crystallographic direction of Mn_3O_4. Two distinct temperature regimes can be identified in Fig. 1(b): (i) $T > T_2 = 33$ K. Above the cell-doubling commensurate magnetic transition at $T_2 = 33$ K,

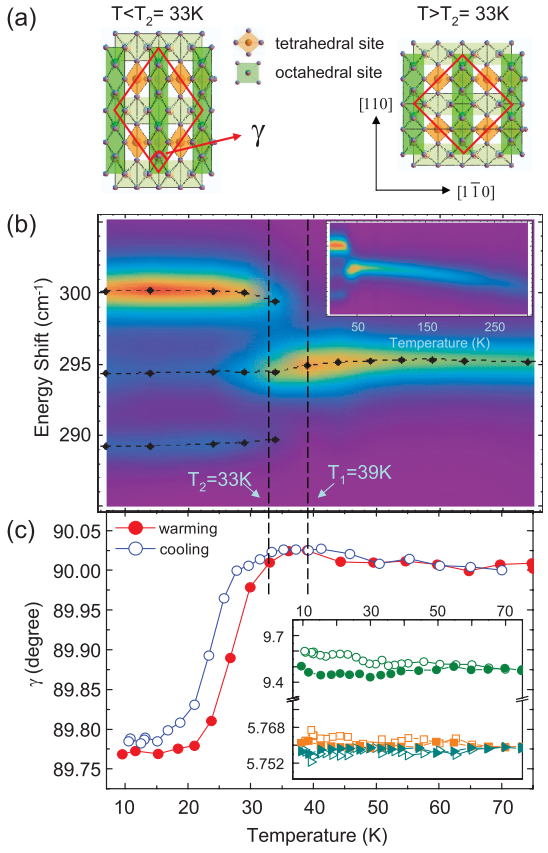

FIG. 1 (color). (a) Illustrations of Mn_3O_4 in the monoclinic ($T < T_2 = 33$ K) and tetragonal ($T > T_2 = 33$ K) stuctures. (b) Contour plot of the T_{2g} phonon mode intensity as functions of energy and increasing temperature; red, 700 counts; blue, 0 counts. (inset) Contour plot of the T_{2g} phonon mode intensity between 7–290 K. (c) Temperature dependence of γ—the angle between the a- and b-axis directions—as functions of increasing temperature (closed symbols) and decreasing temperature (open symbols). (inset) Temperature dependence [in K] of lattice constants a (squares), b (triangles), and c (circles) [in Å] for Mn_3O_4 with increasing (closed symbols) and decreasing (open symbols) temperature.

the T_{2g} mode exhibits conventional behavior: with decreasing temperature from 290 to 33 K, this mode narrows and shifts from ~290 to ~295 cm^{-1} in a manner consistent with anharmonic (multiphonon) effects [15] [see inset, Fig. 1(b)]. Although there is a slight decrease in the T_{2g} mode frequency in the incommensurate magnetic phase regime between $T_2 = 33$ K and $T_1 = 39$ K, presumably due to magnetoelastic effects, this mode exhibits no evidence for a change in structural symmetry above $T_2 = 33$ K. (ii) $T < T_2 = 33$ K. Below the cell-doubling commensurate magnetic transition $T_2 = 33$ K, the T_{2g} mode abruptly splits into two modes near 290 cm^{-1} and 300 cm^{-1}. This splitting is consistent with a tetragonal-to-monoclinic distortion below T_2, which splits the degenerate T_{2g} mode by expanding the $Mn^{2+} - O^{2-}$ bond length along the easy-axis [110] direction and contracting the $Mn^{2+} - O^{2-}$ bond length along the $[1\bar{1}0]$ direction [see illustrations, Fig. 1(a)]. The relative intensities of the modes shown in Fig. 1(b) for $T < T_2$ confirm that the $Mn^{2+} - O^{2-}$ bond length expands along the easy-axis [110] direction below $T_2 = 33$ K: the higher-energy (~300 cm^{-1}) split mode—associated with vibrations of the contracted $Mn^{2+} - O^{2-}$ bond—exhibits the strongest light scattering intensity, indicating that the contracted $Mn^{2+} - O^{2-}$ bond is oriented in the direction of the incident light polarization, i.e., along the $[1\bar{1}0]$ direction. By contrast, the intensity of the lower-energy (~290 cm^{-1}) split mode—associated with vibrations of the expanded $Mn^{2+} - O^{2-}$ bond—has a substantially weaker intensity than the 300 cm^{-1} split mode, indicating that the expanded $Mn^{2+} - O^{2-}$ bond is oriented perpendicular to the incident light polarization, i.e., along the [110] direction.

To provide more definitive evidence for a tetragonal-to-monoclinic phase transition below T_2 in Mn_3O_4, we used x-ray diffraction to study a number of Bragg reflections; in particular, we measured the temperature dependence of the θ, 2θ, ϕ, and χ angles of the (440) and (231) Bragg reflections. From these data, we deduced the temperature dependence—on both cooling and warming—of the lattice parameters a, b, c, as well as γ—the angle between the a and b axis [see Fig. 1(c)]. While γ exhibits an abrupt decrease near $T_2 = 33$ K, the a- and b-axis lattice parameters exhibit no significant temperature dependence, and the c-axis lattice parameter exhibits only a weak temperature dependence, and hysteretic behavior. These results confirm that Mn_3O_4 exhibits a first-order tetragonal-to-monoclinic structural phase transition near $T_2 = 33$ K, as illustrated schematically in Fig. 1(a). Notably, this result disagrees with the interpretation of earlier powder x-ray diffraction measurements of Mn_3O_4 by Boucher *et al.*, who identified the low temperature structural phase of Mn_3O_4 as tetragonal [16]. However, powder diffraction measurements are less sensitive than our single-crystal diffraction measurements to the observation of a transition to a monoclinic phase, which involves a change in the angle between a- and b-axis directions, but no change in the lattice parameters.

The application of a magnetic field along different crystallographic directions in the ferrimagnetic phase of Mn_3O_4 provides a means of either enhancing the magnetic ordering tendencies of Mn_3O_4—for fields applied along the easy-axis [110] direction—or *frustrating* those ordering tendencies—for fields applied *transverse* to the [110] direction. For example, Figs. 2(a) and 2(c) show that, in the incommensurate magnetic phase regime $T_2 = 33\ \mathrm{K} < T \leq T_1 = 39\ \mathrm{K}$, the 295 cm^{-1} mode associated with the undistorted tetragonal phase [structure II in Fig. 2(b)] exhibits a field-induced splitting similar to that induced upon cooling below $T_2 = 33$ K in zero magnetic field [Fig. 1(b)]. Thus, in the incommensurate magnetic phase, an applied magnetic field along the [110] direction generates a tetragonal-to-monoclinic distortion in Mn_3O_4 by inducing the cell-doubled ferrimagnetic structure associated with the monoclinic phase [Fig. 2(b)]. This strong magnetoelastic response likely arises from a field-induced increase—via spin-orbital coupling—in the hybridization between the $d_{3z^2-r^2}$ and d_{xy} orbitals of (octahedral) Mn^{3+} for $\mathbf{H} \parallel [110]$. Figure 2(d) summarizes the different magnetic and structural phases of Mn_3O_4 as functions of magnetic field and temperature for $\mathbf{H} \parallel [110]$.

More interesting is the magnetostructural phase diagram that results when applying the magnetic field in a direction *transverse* to the ferrimagnetic moment, $\mathbf{H} \parallel [1\bar{1}0]$, i.e., in a direction that places the applied field in competition with the internal field in Mn_3O_4. Figures 3(a) and 3(c) show that three different phase regimes are apparent for this magnetic field orientation at $T = 7\ \mathrm{K} (\ll T_2)$. In the low-field regime, i.e., for $H < 1T$ and $T \ll T_2$, the phonon spectrum is identical to that observed at zero field and low temperatures in Mn_3O_4, indicative of a monoclinic ferrimagnetic phase with the Mn spins oriented in the [110] direction [structure I in Fig. 3(b)]. On the other hand, in the high-

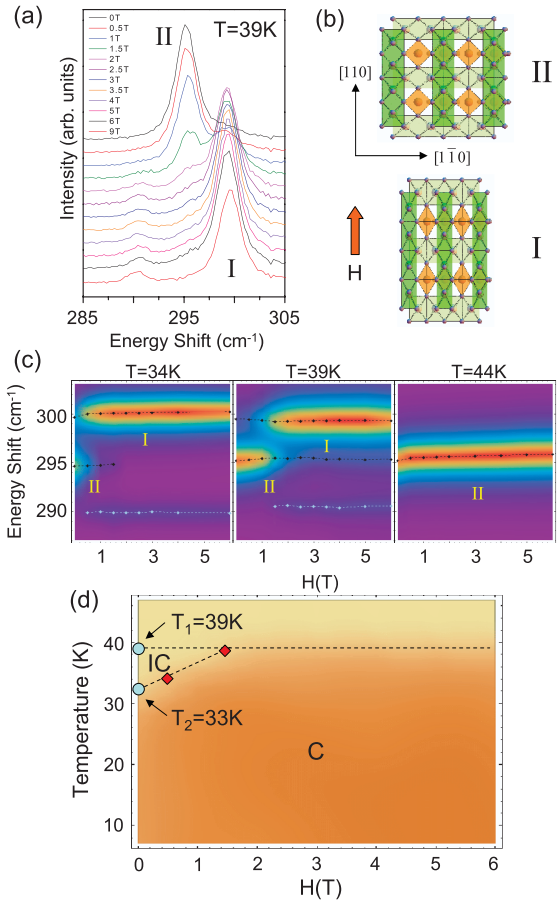

FIG. 2 (color). (a) Field dependence of the Raman spectra at $T = 39$ K for $\mathbf{H} \parallel [110]$. (b) Illustrations of the Mn_3O_4 structure in (top) the low-field undistorted phase and (bottom) the high-field monoclinic phase. (c) Intensities of the split phonon modes as functions of energy and field at (left) $T = 34$ K, (middle) 39 K, and (right) 44 K; red, 700 counts; blue, 0 counts. (d) $H - T$ phase diagram for $\mathbf{H} \parallel [110]$; orange, structure I; yellow, structure II; IC, incommensurate magnetic phase; C, commensurate (cell-doubled) magnetic phase.

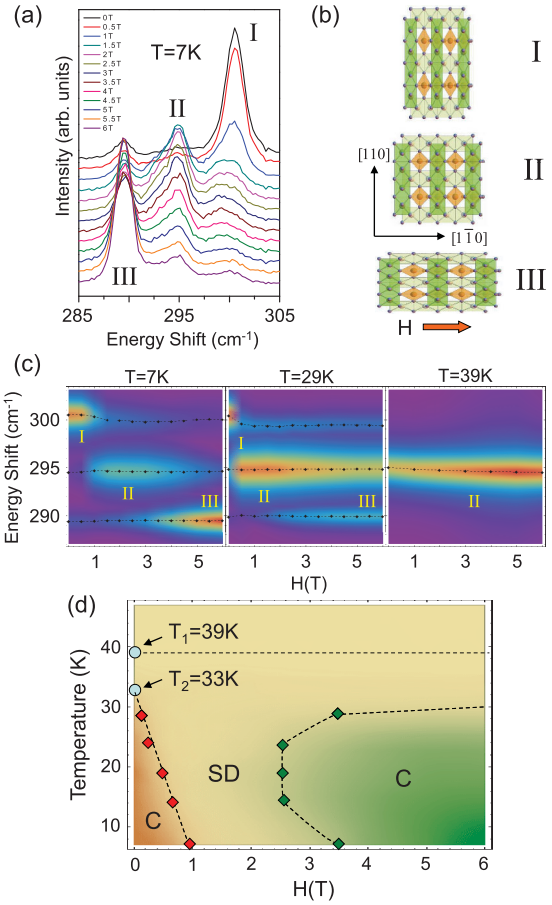

FIG. 3 (color). (a) Field dependence of the Raman spectra at $T = 7$ K for $\mathbf{H} \parallel [1\bar{1}0]$. (b) Illustrations of the Mn_3O_4 structure in (top) the low-field monoclinic phase, (middle) intermediate undistorted tetragonal phase, and (bottom) high-field monoclinic phases. (c) Intensities of the split phonon modes as functions of energy and field at (left) $T = 7$ K, (middle) 29 K, and (right) 39 K; red, 700 counts; blue, 0 counts. (d) $H - T$ phase diagram for $\mathbf{H} \parallel [1\bar{1}0]$; orange, structure I; yellow, structure II; green, structure III; *SD*, spin disordered; and *C*, commensurate (cell-doubled) magnetic phase.

field regime, i.e., for $H > 4T$ and $T \ll T_2$, the lowest energy T_{2g} phonon is split into distinct modes near 290 and 300 cm^{-1}, but the lower-energy 290 cm^{-1} split mode—associated with vibrations of the expanded $Mn^{2+} - O^{2-}$ bond—has greater scattering intensity than the 300 cm^{-1} split mode. This spectrum indicates that the expanded $Mn^{2+} - O^{2-}$ bond, and therefore the Mn spins, are reoriented by the applied field along the applied field direction, i.e., along the $[1\bar{1}0]$ direction [structure III in Fig. 3(b)].

Most remarkable, however, is the intermediate-field regime, i.e., $1T < H < 4T$ and $T \ll T_2$, with $\mathbf{H} \parallel [1\bar{1}0]$, shown in Figs. 3(a) and 3(c): in this regime, the phonon spectrum is the same as that in the paramagnetic tetragonal phase, i.e., the dominant mode is the ~295 $cm^{-1} T_{2g}$ phonon associated with structure II in Figs. 3(b). Thus, in this field range, Mn_3O_4 adopts a symmetric (tetragonal) structural configuration, in order to resolve the frustration imposed on the Mn spins by the competing internal ($\mathbf{M} \parallel [110]$) and transverse external ($\mathbf{H} \parallel [1\bar{1}0]$) fields. This field-induced tetragonal configuration is expected to be associated with a disordered spin state near $T \sim 0$—similar to that observed in the high temperature paramagnetic phase—because of the degeneracy between [110] and $[1\bar{1}0]$ Mn spin orientations in this structural phase. Indeed, magnetization measurements of Mn_3O_4 by Dwight and Menyuk showed that the application of a ~1 T field transverse to the easy-axis direction of Mn_3O_4 at 4.2 K results in slow spin relaxation processes consistent with a disordered spin system [17]. The full $H - T$ phase diagram for Mn_3O_4 with $\mathbf{H} \parallel [1\bar{1}0]$ inferred from our Raman results is summarized in Fig. 3(d).

What are the main lessons of the rich field-induced magnetostructural phases observed here in Mn_3O_4? The most significant result is the observation of a quantum phase transition to an intermediate-field, spin-orbital frustrated state at $T \sim 0$ for $\mathbf{H} \parallel [1\bar{1}0]$. This result reveals a novel mechanism for frustrating spin–orbital-order at $T \sim 0$: the balancing of elastic and magnetic energies in the presence of a transverse applied field in Mn_3O_4 favors a transition to a more symmetric structural configuration that protects the spin-orbital degeneracy over a wide field range. Hydrostatic pressure frustrates orbital order similarly, by creating more symmetric structural configurations [18]. Similar field-tuned frustrated phases should be observable in other materials with strong magnetoelastic coupling, such as MnV_2O_4 [10]. Second, our results show that the rich magnetodielectric and magnetoelastic effects in Mn_3O_4 [19] are associated with the field-induced manipulation of tetragonal-to-monoclinic phase changes, caused by tuning the hybridization between the $d_{3z^2-r^2}$ and d_{xy} orbitals of octahedral Mn^{3+}. Finally, our results identify Mn_3O_4 as a particularly simple, model system in which to study a rare state of matter—a field-tuned $T \sim 0$ spin-orbital frustrated phase—that is accessible without introducing disorder. Field-dependent heat capacity measurements of Mn_3O_4 would be useful for studying the change in entropy in the spin-orbital frustrated phase—e.g., to test whether this state is a quantum spin liquid. Neutron scattering studies are also needed to explore the field-dependent evolution of spin dynamics in the spin-orbital frustrated phase of Mn_3O_4, e.g., to look for evidence of quantum criticality, such as ω/T scaling of the spin excitations, and to compare with unconventional spin dynamics observed near magnetic order-disorder phase transitions in other systems, such as quasi-one-dimensional $CoNb_2O_6$ [20].

This material is based on work supported by the U.S. Department of Energy, Division of Materials Sciences, under DE-FG02-07ER46453, through the Frederick Seitz Materials Research Laboratory at the University of Illinois at Urbana-Champaign, and by the National Science Foundation under Grant No. NSF DMR 08-56321.

[1] M. Imada, A. Fujimori, and Y. Tokura, Rev. Mod. Phys. **70**, 1039 (1998).
[2] L. F. Feiner, A. M. Oles, and J. Zaanen, Phys. Rev. Lett. **78**, 2799 (1997).
[3] V. Tsurkan *et al.*, J. Phys. Chem. Solids **66**, 2036 (2005).
[4] B. Canals and C. Lacroix, Phys. Rev. Lett. **80**, 2933 (1998).
[5] N. Büttgen *et al.*, New J. Phys. **6**, 191 (2004).
[6] A. P. Ramirez *et al.*, Nature (London) **399**, 333 (1999).
[7] S. B. Lee and L. Balents, Phys. Rev. B **78**, 144417 (2008).
[8] S.-H. Lee *et al.*, Phys. Rev. Lett. **84**, 3718 (2000); A. B. Sushkov *et al.*, Phys. Rev. Lett. **94**, 137202 (2005); M. Matsuda *et al.*, Nature Phys. **3**, 397 (2007).
[9] M. Onoda and J. Hasegawa, J. Phys. Condens. Matter **15**, L95 (2003); H. Tsunetsugu and Y. Motome, Phys. Rev. B **68**, 060405(R) (2003); S.-H. Lee *et al.*, Phys. Rev. Lett. **93**, 156407 (2004); T. Suzuki *et al.*, Phys. Rev. Lett. **98**, 127203 (2007).
[10] J.-H. Chung *et al.*, Phys. Rev. B **77**, 054412 (2008).
[11] G. B. Jensen and O. V. Nielsen, J. Phys. C **7**, 409 (1974).
[12] B. Chardon and F. Vigneron, J. Magn. Magn. Mater. **58**, 128 (1986).
[13] J. F. Karpus *et al.*, Phys. Rev. Lett. **93**, 167205 (2004).
[14] C. M. Julien and M. Massot, J. Phys. Condens. Matter **15**, 3151 (2003); B. Ammundsen *et al.*, J. Phys. Chem. B **103**, 5175 (1999); L. Malavasi *et al.*, Phys. Chem. Chem. Phys. **4**, 3876 (2002); following these references we use the cubic space group notation to index the Raman-active phonons in tetragonal Mn_3O_4.
[15] D. Mihailovic, K. F. McCarty, and D. S. Ginley, Phys. Rev. B **47**, 8910 (1993).
[16] B. Boucher, R. Buhl, and M. Perrin, J. Phys. Chem. Solids **32**, 2429 (1971).
[17] K. Dwight and N. Menyuk, Phys. Rev. **119**, 1470 (1960).
[18] F. Nakamura *et al.*, Phys. Rev. B **65**, 220402(R) (2002); P. Steffens *et al.*, Phys. Rev. B **72**, 094104 (2005).
[19] T. Suzuki and T. Katsufuji, Phys. Rev. B **77**, 220402(R) (2008); R. Tackett *et al.*, Phys. Rev. B **76**, 024409 (2007).
[20] R. Coldea *et al.*, Science **327**, 177 (2010).